

Hydrodynamic instabilities in axisymmetric geometry

Self-similar models and numerical simulations

J. Breil,* L. Hallo, P.H. Maire, and M. Olazabal-Loumé

Centre Lasers Intenses et Applications, UMR 5107 CEA - CNRS - Université de Bordeaux 1, Université Bordeaux 1, 33405 Talence Cedex, France

Hydrodynamic instabilities play an important role in the target compression for inertial confinement fusion (ICF). We present the analytical solution of a perturbed isentropic implosion. We compare the analytical solution to the results obtained with perturbation and 2D Lagrangian hydrodynamic codes. We also compare results from 2D code and perturbation code on a ICF like test case.

Keywords: hydrodynamic; axisymmetric; linear instabilities

I. INTRODUCTION

The performance of direct drive high yield targets may be severely limited by hydrodynamic instabilities. The implosion process is generally achieved with a sequence of shocks emerging from the ablator to the fuel in the target. It is known that in order to optimize the fuel compression at the end of implosion process, a specific sequence of shocks is required, which must be as close as possible to an isentropic compression. The hot spot quality is also limited by the growth of Richtmyer-Meshkov and Rayleigh-Taylor instabilities around the ablator interface. In order to understand and modelize such instabilities, two complementary numerical approaches are used in this paper. The first is dedicated to the study of linear stability of unsteady complex flows. The code calculates the basic one-dimensional solution and first order three-dimensional perturbations. It is a so-called perturbation code, named Pansy (6). The second is a two-dimensional Lagrangian hydro-code, named CHIC, based on a new cell-centered scheme with a Godunov type solver. Two test cases have been chosen in order to demonstrate the ability of this new numerical method to simulate unstable flows. The first is the modelization of both base and perturbed flows in the linear regime. It is a converging cumulative flow in spherical geometry. An analytical solution can be derived for the behaviour of both stable (internal interface) and unstable (external interface), and obviously for the base flow. We will present analytical solutions for the base flow and for the perturbations in a spherical geometry. These solutions will allow us to understand the effects of aspect ratio and compressibility during implosion.

The second is an ICF like test case which involves only hydrodynamic. We consider a shell with a light fuel in the center and a heavy fuel that surrounds it. The implosion is driven by an external pressure derived from scaling laws. Laser intensity is such that the final pressure is

around 25 Mbar. Analytical solutions are not available in this case since we consider the complex combination of rippled converging shocks and Richtmyer-Meshkov like instabilities occurring at heavy-light fuel interface.

II. PERTURBATION CODE PANSY

The code PANSY (3; 6), calculates the time development of three-dimensional modes of coupled hydrodynamic, thermodynamic, and transport phenomena, including heat flow, viscosity, fully linearized about zero order spherically or cylindrically symmetric compressible flows. The zero order solutions are calculated on a typical one-dimensional (1D) Lagrangian grid and have the form $f^j(t)$, where the f 's are all of the necessary hydrodynamic and other variables, including zone radius and velocity, and where j is the radial zone index. First order quantities, of the form $f_{l,m}^j(t)Y_{l,m}(\theta)\exp[i\varphi]$ for spherical or $f_{k,m}^j(t)\exp[i(kz + m\theta)]$ for cylindrical geometry, are calculated with difference equations which are linearly perturbed forms of the already radially discretized zero order equations, rather than discretizations of the linearly perturbed continuous zero order equations. This relatively conservative/Hamiltonian doctrine produces considerably improved treatment of phenomena requiring high radial resolution, especially artificial viscosity for shocks.

III. HYDRODYNAMIC CODE CHIC

The numerical method in CHIC is based on a new scheme. This scheme uses a cell centered discretisation based on a total energy formulation. The vertices velocity and the fluxes are evaluated using a nodal solver. This solver has been built from conservation arguments and one entropy inequality. It can be viewed as a two-dimensional extension of the acoustic Godunov's solver. This method fully answers an important question concerning Lagrangian hydrodynamic : vertices displacements are made consistent with face fluxes. This method

*Electronic address: breil@celia.u-bordeaux.fr

is currently the subject of a publication (1).

IV. AN ANALYTICAL MODEL FOR LINEAR PERTURBATIONS OF KIDDER'S SELF-SIMILAR SOLUTION

We briefly recall the main features of Kidder's isentropic implosion of a perfect gas (5) which is a special case of selfsimilar cumulative flows in convergent geometries. This 1D solution will be used as our base flow. Let $R(r, t)$ be the radius of a fluid particle at time t which was initially at r . We build the self-similar solution using $R(r, t) = h(t) r$ and $P = s \rho^\gamma$ where s is a constant and $h(t)$ a function to determine. Finally after variable separation one obtains two ODE whose solution is $h(t) = \sqrt{1 - (\frac{t}{\tau})^2}$ where $\tau = \sqrt{\frac{\gamma-1}{2} \frac{r_2^2 - r_1^2}{c_2^2 - c_1^2}}$ is the collapse time, r_1 and r_2 are the internal and external radii, c_1 and c_2 are the isentropic sound speeds located at r_1 and r_2 . The initial density profile is given by (for $r \in [r_1, r_2]$):

$$\rho^0(r) = \left(\frac{r_2^2 - r^2}{r_2^2 - r_1^2} \rho_1^{\gamma-1} + \frac{r^2 - r_1^2}{r_2^2 - r_1^2} \rho_2^{\gamma-1} \right)^{\frac{1}{\gamma-1}}.$$

The isentropic compression is obtained by imposing the following pressure laws at the internal and external interfaces of the domain :

$$\begin{cases} P(R(r_1, t), t) = P_1 h(t)^{-\frac{2\gamma}{\gamma-1}}, \\ P(R(r_2, t), t) = P_2 h(t)^{-\frac{2\gamma}{\gamma-1}}. \end{cases}$$

This fully analytical solution is obtained under the assumption that $\gamma = 1 + 2/\nu$ where $\nu = 1, 2, 3$ whether we have a planar, cylindrical or spherical symmetry. Here we choose $\nu = 3$.

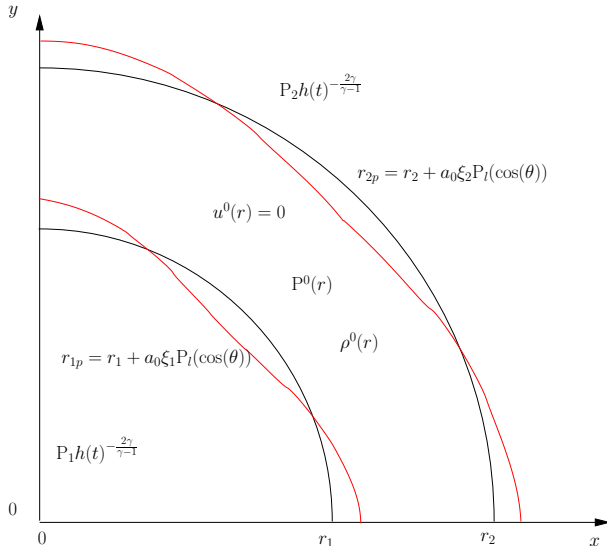


FIG. 1 Perturbation of the shell

We are now going to perturb the internal and external faces of the shell (figure 1) in order to study hydrodynamic instabilities (2; 4). Let $\vec{\xi}(\vec{r}, t)$ be a small displacement around the unperturbed eulerian trajectory $\vec{R}(\vec{r}, t)$. By linearising Euler equations around the base motion, one obtains to first order in $\vec{\xi}(\vec{r}, t)$:

$$(\mathcal{L}) \begin{cases} h^4(t)\tau^2 \frac{d^2 \vec{\xi}}{dt^2} + \vec{r} \operatorname{div}_r \vec{\xi} - \frac{\gamma\tau^2}{\rho^0} \operatorname{grad}_r (P^0 \operatorname{div}_r \vec{\xi}) \\ - \operatorname{grad}_r \vec{\xi} \cdot \vec{r} - \vec{r} \times \operatorname{rot}_r \vec{\xi} = \vec{0}, \end{cases}$$

where \vec{r} denotes the lagrangian position vector, ρ^0 and P^0 are density and pressure of the base motion. In order to solve (\mathcal{L}) , let us introduce $\vec{\xi}(\vec{r}, t) = \vec{X}(\vec{r})G(t)$. After some rearrangement, we find for $t \in [0, \tau[$ and $r \in [r_1, r_2]$:

$$(\mathcal{T}) h^4(t)\tau^2 \frac{d^2 G}{dt^2} + \mu G(t) = 0,$$

$$(\mathcal{S}) (\mu-1)\vec{X} + (\gamma-1)\sigma\vec{r} + \frac{\gamma\tau^2 P}{\rho} \operatorname{grad}_r \sigma + \operatorname{grad}_r(\vec{r} \cdot \vec{X}) = \vec{0},$$

where $\sigma = \operatorname{div}_r \vec{X}$ and μ is a separation constant. We impose the initial values $G(0) = 1$ and $\frac{dG}{dt}(0) = 0$, then (\mathcal{S}) is solved under incompressibility assumption, i.e. $\sigma = 0$. Therefore thanks to (\mathcal{S}) , $\operatorname{rot}_r \vec{X} = \vec{0}$, hence $\vec{X} = \operatorname{grad}_r \Phi$ where $\Phi(r, \theta)$ satisfies the Laplace equation

$$\frac{1}{r^2} \frac{\partial}{\partial r} \left(r^2 \frac{\partial \Phi}{\partial r} \right) + \frac{1}{r^2 \sin(\theta)} \frac{\partial}{\partial \theta} \left(\sin(\theta) \frac{\partial \Phi}{\partial \theta} \right) = 0,$$

which admits, after variable separation, two fundamental solutions : $\Phi_1 = r^{-(l+1)} P_l(\cos(\theta))$ and $\Phi_2 = r^l P_l(\cos(\theta))$ with $l \in \mathbb{N}$ and P_l Legendre polynomial. Then we define the two fundamental solutions of (\mathcal{S}) : $\vec{X}_1 = \operatorname{grad}_r \Phi_1$ with $\mu_1 = l + 2$ and $\vec{X}_2 = \operatorname{grad}_r \Phi_2$ with $\mu_2 = -l + 1$. After time scaling ($t \rightarrow t/\tau$), we solve the two evolution equations for G_1 with μ_1 and for G_2 with μ_2 :

$$\begin{cases} G_1(t) = \sqrt{1-t^2} \cos \left[\frac{\sqrt{l+1}}{2} \log \left(\frac{1-t}{1+t} \right) \right], \\ G_2(t) = \frac{1}{2} \sqrt{1-t^2} \left[\left(\frac{1-t}{1+t} \right)^{\frac{\sqrt{l}}{2}} + \left(\frac{1+t}{1-t} \right)^{\frac{\sqrt{l}}{2}} \right]. \end{cases}$$

We notice that $\lim_{t \rightarrow 1^-} G_1(t) = 0$ and for $l > 1$ $\lim_{t \rightarrow 1^-} G_2(t) = +\infty$. The time evolution of amplification for the point with initial radius r and $\theta = 0$ is given by

$$\xi_r(r, t) = -A_1(l+1)r^{-l-2}G_1(t) + A_2lr^{l-1}G_2(t),$$

where the constants A_1, A_2 are determined by the initial levels of perturbations ξ_1 and ξ_2 at r_1 and r_2 , following

$$\begin{cases} -(l+1)r_1^{-l-2}A_1 + lr_1^{l-1}A_2 = \xi_1, \\ -(l+1)r_2^{-l-2}A_1 + lr_2^{l-1}A_2 = \xi_2. \end{cases}$$

V. NUMERICAL RESULTS

In the cumulative converging test case, the external interface is unstable, as it has been previously shown, whereas the internal interface is stable. This situation is similar to the one of Rayleigh-Taylor instability in planar geometry. The main goals to be achieved are :

- a proper evaluation of the perturbation amplification at the external interface for low l mode numbers where an important amplification is predicted by the analytical model.
- Knowing that the internal interface is stable but oscillating, an aspect ratio effect can be expected. This point is confirmed by the analytical solution : for example with $\xi_1 = 2.848738$ and $\xi_2 = 1$, we can even stabilize the external interface.

Three configurations are studied here. First of all, initial perturbations of modes $l = 4$ and $l = 8$ have been applied to the external interface with an amplitude $\xi_1 = 0$ and $\xi_2 = 1$. In order to ensure a linear regime for CHIC direct 2D simulations, an effective initial amplitude $a_0 = 10^{-6}$ has been used. This amplitude is largely below the non-linear criteria $a_0 l/r \ll 1$. This numerical artefact is not necessary for the perturbation code PANSY since base flow is not coupled with perturbations. The results will be normalized.

In all cases we use $a_0 = 10^{-6}$, $r_1 = 0.9$, $r_2 = 1$, $P_1 = 0.1$, $P_2 = 10$ and $\rho_2 = 10^{-2}$. From this we get $\rho_1 = 10^{-3}$, $s = 10^5$ and $\tau = 7.265 \cdot 10^{-3}$. The computational domain is defined using the symmetries of the mode 8 i.e. $(r, \theta) \in [r_1, r_2] \times [0, \frac{\pi}{2}]$. We use equiangular meshes with $(n_x, n_y) = (25, 44)$, $(n_x, n_y) = (50, 88)$ and $(n_x, n_y) = (100, 176)$. For the perturbation code, we present converged calculations. Figures 2 and 3 show the normalized amplification at external interface for mode $l = 4$ and $l = 8$ respectively. Amplification for perturbation code is superposed with analytical solution. A good agreement can be noticed with 2D solutions. The agreement becomes better and better as the mesh is refined.

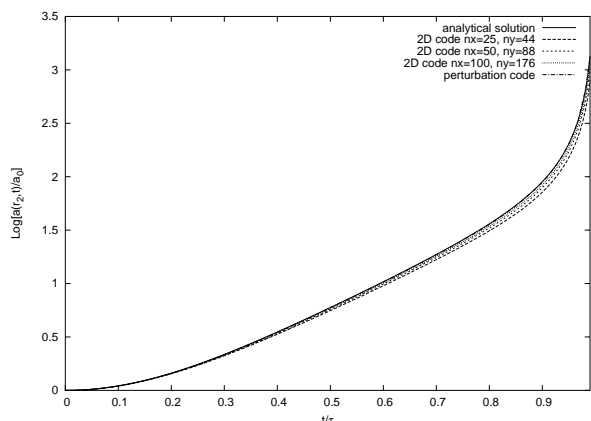


FIG. 2 mode $l = 4$, $\xi_1 = 0$, $\xi_2 = 1$, $r = r_2$

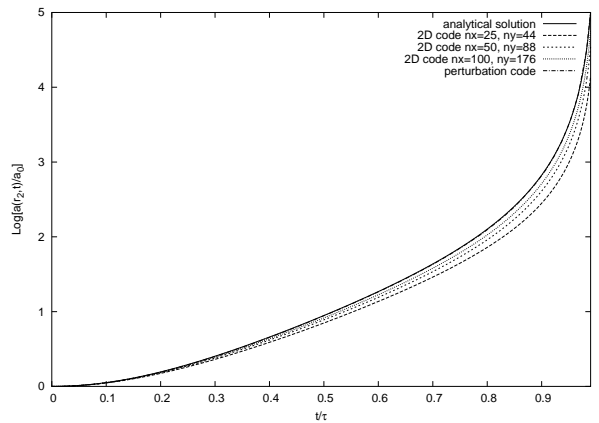


FIG. 3 mode $l = 8$, $\xi_1 = 0$, $\xi_2 = 1$, $r = r_2$

At last we focus on the coupled test case presented below. We use the previous numerical values but with $\xi_1 = 2.848738$ and $\xi_2 = 1$. This configuration becomes very difficult due to the aspect ratio between internal and external interface. External perturbation amplification presented on figure 5 is not only reduced, as compared to previous case (figure 3), but goes back to its initial value at final time. The 2D code predictions are correct up to time $t = 0.6 \tau$, after which the calculated perturbations become larger than the theoretical one. The behaviour can be improved by using a refined mesh. As the spatial differencing used here is only first order accurate, large meshes are required in order to achieve convergence. Similar behaviour is found on the internal interface perturbation which is presented in figure 4.

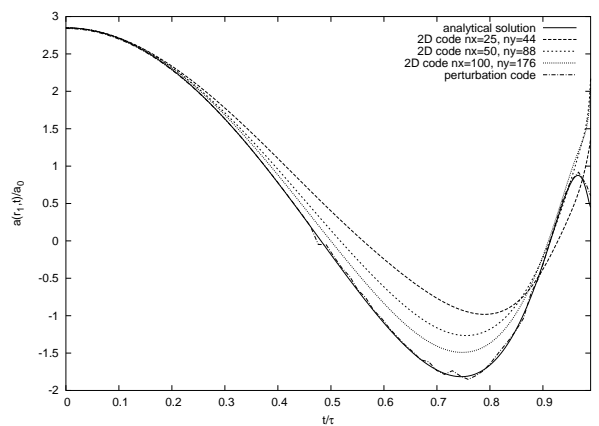


FIG. 4 mode $l = 8$, $\xi_1 = 2.848738$, $\xi_2 = 1$, $r = r_1$

VI. PERTURBED TARGET IMPLOSION

Here we treat an ICF like test case. Since thermal conduction and energy laser deposit are not available at this time, in our code an equivalent hydrodynamic test case has been constructed from NIF data. Thus dimensions

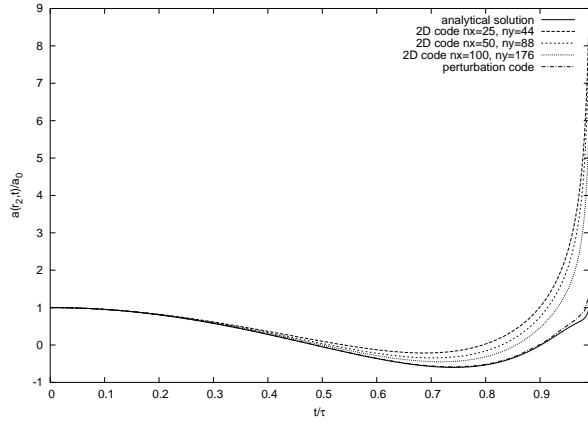


FIG. 5 mode $l = 8$, $\xi_1 = 2.848738$, $\xi_2 = 1$, $r = r_2$

are preserved and a driving pressure is imposed from scaling law. The shell is spherical. The external radius is $1,1 \text{ mm}$ and the interface between heavy/light material is located at $r = 1 \text{ mm}$, as it is shown on figure 8. The initial densities in the shell are such that $\rho_{heavy} = 1 \text{ g/cm}^3$ and $\rho_{heavy}/\rho_{light} = 100$. Initial pressure is set to 25 bar .

If we assume an ideal gas law for the material, a Chapman-Jouguet kinetic closure for ablation front, we can exhibit that pressure at ablation front has to evolve as :

$$P_{abl} = 2 \rho_c^{1/3} (I/4)^{2/3}$$

where I is the incident driver intensity in Tw/cm^2 and P_{abl} in Mbar . The driving pressure is presented on figure 7 from the driving intensity presented on figure 6. This driving pressure law will produce a sequence of waves in the shell such that focalisation time is $\tau = 12 \text{ ns}$. What we are interested here in is Richtmyer-Meshkov like instability amplification which will occur at the heavy/light interface. For this test case no analytical solution exists but PANSY code will give the reference solution. This code has been widely used on such kind of problems.

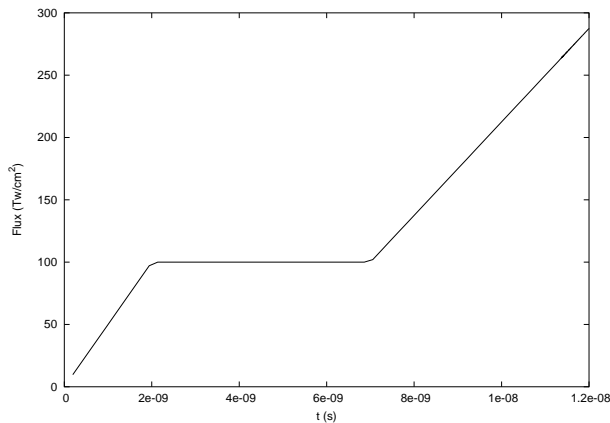


FIG. 6 Driving intensity law

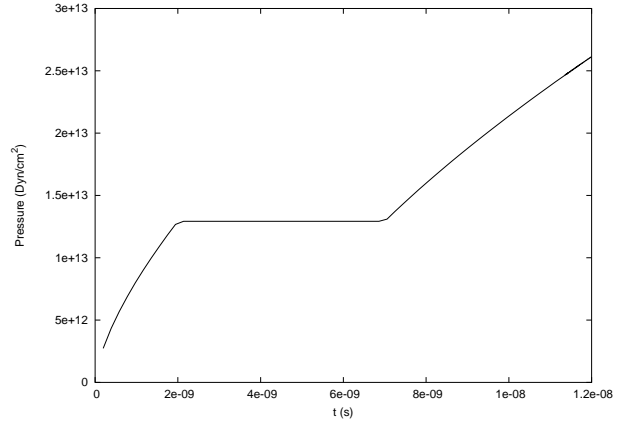


FIG. 7 Driving pressure law

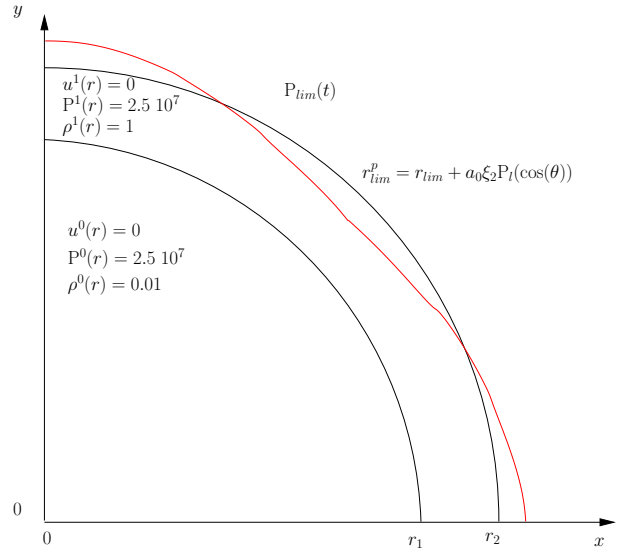


FIG. 8 Initial perturbation of the shell

Concerning initial perturbations, we will use a $l = 4$ mode representative of laser beam non-uniformity. As we show on the homogeneous cumulative flow the mode $l = 4$ has a large spatial extension and does not require a very stretched mesh compare to the base flow. The main drawback is the coupling of perturbation which makes this test case difficult and interesting.

First of all we present the perturbation and density profiles on figure 9. The perturbation imposed initially at the external interface has been transported by the first shock up to the heavy/light interface which was initially not perturbed. At time $t = 3.2 \text{ ns}$, the perturbation is imprinted on the internal interface and grows in the meantime. A Richtmyer-Meshkov like instability should develop at this interface with an inversion of perturbation phase. In fact, for $l = 4$ the perturbed shock travelling in the light material is not unstable but only slightly decreases and continuously feed the interface perturbation. At time $t = 9.5 \text{ ns}$ a second shock arising from disconti-

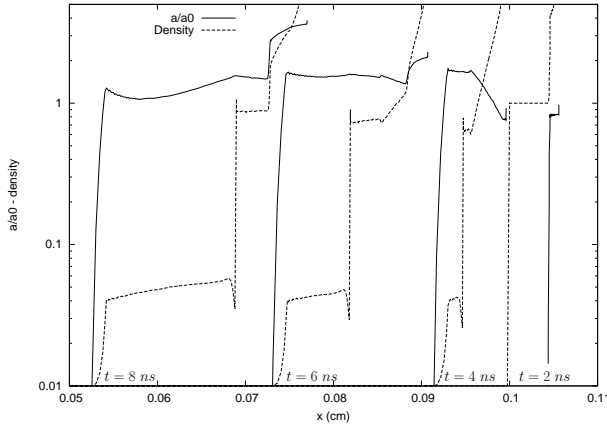


FIG. 9 Perturbation and density profiles for $t = 2ns$, $t = 4ns$, $t = 6ns$ and $t = 8ns$ (PANSY result)

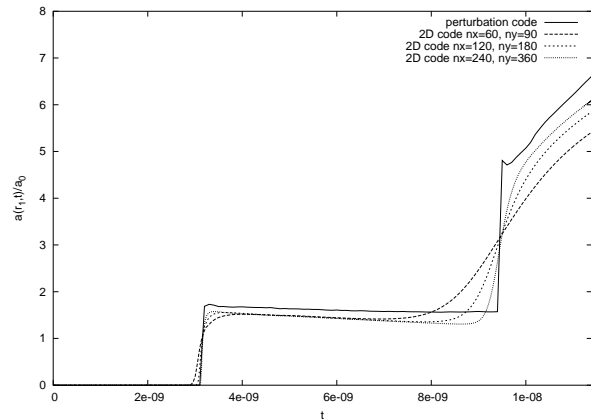


FIG. 10 Normalized amplification versus time at heavy/light interface

nunity in driving pressure law generates a second imprint on the heavy/light interface. This perturbed shock has a larger velocity and intensity than the first one which explains the larger level of perturbation transmitted to the interface. As the pressure increases, shocks are launched in the heavy material and accelerate the interface. We observe then a quite linear increase of the perturbation amplitude at the interface relative to a kind of Richtmyer-Meshkov instability. Finally, we present normalized amplification versus time at heavy/light interface on figure 10. The 2D results from CHIC first order spatial accuracy simulations are in good agreement with PANSY results which is second order accurate. Chronometry is

exactly the same for base flow. Concerning perturbation we can notice that the first imprint perturbation does not reach the reference solution. The relative imprint difference is less than 10%. The amplitude decrease after the first shock is well reproduced as well as the amplification up to final time. The second shock interaction is clearly less accurately calculated than the first one, which can be explained by the lack of accuracy of first order method. This problem can be solved using a larger number of discretisation cells. Spatial convergence is observed clearly on figure 10.

VII. CONCLUSION

Linear perturbation growth in converging geometries have been studied. The simulations have been performed using the 2D hydrodynamic code CHIC actually developed at CELIA laboratory and the perturbation code PANSY. We have presented a fully analytical solution of the perturbed Kidder isentropic implosion in spherical geometry. The comparison of our results from both codes with the analytical solution shows a good agreement. In a second time, we set up an ICF like hydrodynamic test case. Here the perturbation code gives us the reference solution due to the lack of theoretical results. Simulations show a good behaviour of the 2D code compared with the perturbation code results.

References

- [1] R. ABGRALL, J. BREIL, P.H. MAIRE, J. OVADIA *A Lagrangian scheme for multidimensional compressible flow* submitted to J. Compu. Phys.
- [2] J. BREIL, L. HALLO, P.-H. MAIRE, M. OLAZABAL-LOUMÉ *Hydrodynamic instabilities in cylindrical geometry self-similar models and numerical simulations* 31st EPS Conference on Plasma Physics, London (2004).
- [3] L. HALLO ET AL. *Modeling of linear perturbation growth in gas dynamics: from incompressible to compressible flows* 6th IWPCMTM Marseille, (1997).
- [4] S.J. HAN AND B.R. SUYDAM *Hydrodynamic instabilities in an imploding cylindrical plasma shell* Phys. Review A **26**,926-939, (1982).
- [5] R. E. KIDDER *Laser-driven compression of hollow shells : power requirements and stability limitations* Nuclear Fusion **1**,3-14 (1976).
- [6] R.L. MACCRORY ET AL. *Ablation Stability of Laser-Driven Implosions* Nucl. Sci. and Eng. **64**, (1977).